Peer-reviewed version available at *J. Compos. Sci.* **2017**, *1*, , 4; doi:10.3390/jcs1010004

The Induced Stress Field in Cracked Composites by Heat Flow

Jacob Aboudi

School of Mechanical Engineering

Faculty of Engineering,

Tel Aviv University,

Ramat Aviv 69978, Israel

E-mail: aboudi@eng.tau.ac.il, tel: +972-3-6408131, fax: +972-3-6407617

A multiscale (micro-macro) approach is proposed for the establishment of the full thermal and induced stress fields in cracked composites that are subjected to heat flow. Both the temperature and stresses distributions are determined by the solution of a boundary value problem with one-way coupling. In the micro level and for combined thermomechanical loading, a micromechanical analysis is employed to determine the effective moduli, coefficients of thermal expansion and thermal conductivities of the undamaged composite. In the macro level, the representative cell method is employed according to which the periodic damaged composite region is reduced, in conjunction with the discrete Fourier transform, to a finite domain problem. As a result, a boundary value problem is obtained in the Fourier transform domain which is appropriately discretized and solved. The inverse transform and an iterative procedure provide the full thermal and stress fields. The proposed method is verified by comparisons with exact solutions. Applications are given for the determination of the thermal and stress fields in cracked fiber-reinforced polymeric composite, cracked porous ceramic material and cracked periodically layered ceramic composite caused by the application of heat flow. The presented formulation admits however the application of a combined mechanical and heat flux on cracked composites.

Keywords : fiber-reinforced composites; porous materials; thermal stresses; repre-sentative cell method; high-fidelity generalized method of cells

There are many books, review articles and papers that are dedicated to the investigation of the behavior of cracked solids and composites that are subjected to mechanical loadings. A relatively few papers appeared concerning the induced thermal stresses caused by the application of heat flow in the presence of cracks and other types of damage. Quantifying these stresses in the presence of defects is important as they may give information about the locations of high stress concentrations which can cause failure. It should be mentioned that in the framework of these problems, the temperature field distribution is not constant but rather spatially dependent should be determined according to considered boundary-value problem. The resulting heat flux caused by the application of heat flow in a cracked homogeneous material is singular at the crack front, and the temperature is continuous along the crack line and discontinuous across the crack (insulated crack).

Due to the one-way thermomechanical coupling, the temperature field induces thermal stresses in the material which are singular near the crack tip. Examples of some articles in which the effect of heat flow in cracked materials is investigated are: Koizumi et al. (1979), Wu (1984), Tsai (1984), Sturla and Barber (1988), Kuo (1990), Hwu (1990), Hwu (1992), Tarn and Wang (1993), Itou (2000), Ursescu and Dascalu (2006), Zhong and Wu (2012) and references cited there, and chapter 10 in Hwu (2010) monograph . The analysis of Ting and Yan (1992) of the singularities at the tip of interfacial cracks in anisotropic materials subjected to heat flow forms a generalization of the square root singularity that occurs in homogeneous materials. A recent article in which the extended finite element method has been employed for the simulation of the heat flux and thermal stresses in cracked solids has been presented by Duflot (2007).

The aforementioned investigations concerned with cracks in homogeneous materials or interfacial cracks between two homogeneous materials. When the effect of thermal loading on composite materials with cracks is sought, the application of these analyses necessitates the homogenization of the considered multiphase material. As a result of this homogenization, the effect of the composite's periodic microstructure is lost. Furthermore, when the homogenization technique is employed in the analysis of a cracked composite with periodic microstructure, a repeating unit cell which represents the entire composite is considered. The introduction of a crack

is not a realistic situation.

In the present investigation, a multiscale analysis is proposed for the establishment of the full thermoelastic field caused by the application of remote heat flow on cracked composite materials while taking into account their microstructure distributions. As a result of the application of thermal loading the temperature and heat flux distributions are established by solving the steady state heat equation. The one-way coupling with the mechanical equations induces thermal stresses in the composite which are subsequently determined by solving these equations.

The proposed method of solution consists of a micromechanical analysis which is followed by a macromechanical one. In the most general case of a composite subjected to remote thermo-mechanical loading, the micromechanical analysis provides the effective thermal conductivities, elastic moduli and coefficients of thermal expansion of the undamaged composite. This is carried out by utilizing the high-fidelity generalized method of cells (HFGMC) which has been fully described in Aboudi et al. (2013). In the framework of the macromechanical analysis the representative cell method, Ryvkin and Nuller (1997), is employed. According to this method, the composite domain is divided into several rectangular cells with respect to which the governing and constitutive equations are formulated. This is followed by the application of the discrete Fourier transform which reduces the multiple cells problem to the analysis of a single cell in the transform domain. The transformed temperature and displacement vector are expanded into a second-order polynomial, and the heat and equilibrium equations as well as the interfacial and boundary conditions are imposed in the average (integral) sense. A discretization of the single cell problem provides the solution in the form of a system of algebraic equations, see Aboudi et al. (2013). The inversion of the Fourier transform provides the actual thermal and mechanical fields at the various cells, and thus at every desired point of the composite. The effect of crack existence is taken into account by the continuum damage mechanics considerations combined with the localized damage analysis as described by Aboudi and Ryvkin (2012) and Ryvkin and Aboudi (2012). It should be noted that in both these two articles the constant temperature has been uniformly prescribed in the entire composite.

The proposed approach is verified by comparing its prediction with exact solutions for a crack embedded in homogeneous materials that are subjected to remote heat flow. The temperature

Peer-reviewed version available at J. Compos. Sci. 2017, 1, , 4; doi:10.3390/jcs1010004

fiber-reinforced polymer matrix composite, porous ceramic material and periodically layered ceramic composite, all of which are subjected to heat flow.

The present article is organized as follows. In Section 2, the constitutive and governing equations are presented. This is followed in Section 3 by the method of solution which is presented in the real space followed by its formulation in the Fourier transform domain. The solution in the latter domain utilizes the methods presented in Aboudi et al. (2013). The inversion of the Fourier transform provides the actual solution which requires iterations for convergence. In Section 4, verifications of the proposed method are presented by comparison with exact solutions. Section 5 provide results of the application of the proposed method on three types of composites. Finally, a Conclusion section is given for a summary and future generalizations.

2. Constitutive and Governing Equations

Consider a thermoelastic homogeneous orthotropic material. The constitutive equations are given as follows.

$$\boldsymbol{\sigma} = \boldsymbol{C} : \boldsymbol{\epsilon} - \boldsymbol{\Gamma} T \tag{1}$$

where $\boldsymbol{\sigma}$, $\boldsymbol{\epsilon}$, $\boldsymbol{C}$ and $\boldsymbol{\Gamma}$ are the stress, strain, stiffness and thermal stress tensors, respectively. In this equation, T is the temperature field deviation from a reference temperature. The thermal flux vector $\boldsymbol{q}$ is related to the temperature gradient via the Fourier's law in the form

$$\boldsymbol{q} = -\boldsymbol{\kappa}\, \nabla T \tag{2}$$

and $\boldsymbol{\kappa}$ is the thermal conductivity tensor.

The governing equations are given by

$$\nabla \cdot \boldsymbol{\sigma} = \boldsymbol{0} \tag{3}$$

and

$$\nabla \cdot \boldsymbol{q} = \boldsymbol{0} \tag{4}$$

the latter through the constitutive equation (1) (one-way thermomechanical coupling).

As discussed in Aboudi and Ryvkin (2012), the effect of the crack can be represented, in the framework of the continuum damage mechanics, by introducing a damage parameter D which takes the value of zero or one. In the crack region D=1 whereas D=0 otherwise. As a result Eq. (1) and (2) are reduced to the following form

$$\boldsymbol{\sigma} = (1-D)\boldsymbol{C} : \boldsymbol{\epsilon} - (1-D)\boldsymbol{\Gamma}T \tag{5}$$

and

$$\boldsymbol{q} = -(1-D)\boldsymbol{\kappa}\ \nabla T \tag{6}$$

As discussed in the next section, Eqns. (5) and (6) are more conveniently represented as follows

$$\boldsymbol{\sigma} = \boldsymbol{C} : \boldsymbol{\epsilon} - \boldsymbol{\Gamma}T - \boldsymbol{\sigma}^e \tag{7}$$

$$\boldsymbol{q} = -\boldsymbol{\kappa}\ \nabla T - \boldsymbol{q}^e \tag{8}$$

where

$$\boldsymbol{\sigma}^e = D\left(\boldsymbol{C} : \boldsymbol{\epsilon} - \boldsymbol{\Gamma}T\right) \tag{9}$$

$$\boldsymbol{q}^e = -D\boldsymbol{\kappa}\ \nabla T \tag{10}$$

which play the role of eigenstress and eigen heat flux, respectively. Consequently, the damage parameter D=1 in the crack region results into traction-free and insulated crack surfaces.

3. Method of Solution

Consider a composite material with doubly periodic microstructure. As an illustration, Fig. 1(a) shows a composite with a hexagonal array of fibers embedded in the matrix. Also shown is a crack of length 2a which connects two adjacent fibers. The composite is subjected to a heat

periodicity of the composite is lost and consequently a repeating unit cell (a representative volume element) does not exist. In the following we present a method of solution that is based on the representative cell method, Ryvkin and Nuller (1997), which is capable to establish the full temperature and thermoelastic fields. To this end, let us consider a rectangular domain $-D \leq X_1 \leq D$, $-H \leq X_2 \leq H$ of the composite which includes the crack region. It is assumed that this rectangular domain which is subjected to the heat flux $\bar{\boldsymbol{q}}$ is sufficiently extensive such that the temperature and thermoelastic fields at its boundaries are not influenced by the crack existence. It should be mentioned that as long as the rectangular domain is sufficiently extensive, the distribution of the fibers and the location of the crack is arbitrary. It is advisable however to preserve symmetry (as illustrated by the insets of the figures that are discussed in the following) in order to obtain symmetrical field distributions. Consequently, the boundary conditions (presently the heat flux) that are applied on $X_1 = \pm D$ and $X_2 = \pm H$ can be referred to as the far-field boundary conditions. This region is divided into $(2M_1 + 1) \times (2M_2 + 1)$ cells, see Fig. 1(b) for $M_1 = M_2 = 2$. Every cell is labeled by (K_1, K_2) with $K_1 = -M_1, ..., M_1$ and $K_2 = -M_2, ..., M_2$. In each cell, local coordinates (X_1', X_2') are introduced whose origins are located at its center, see Fig. 1(c).

3.1 Formulation in the real domain

The constitutive equation (7) in cell (K_1, K_2) can be written as

$$\boldsymbol{\sigma}^{(K_1,K_2)} = \boldsymbol{C} : \boldsymbol{\epsilon}^{(K_1,K_2)} - \boldsymbol{\Gamma} T^{(K_1,K_2)} - \boldsymbol{\sigma}^{e(K_1,K_2)} \tag{11}$$

If the crack exists in the cell $(K_1 = 0, K_2 = 0)$ only, it follows that $\boldsymbol{\sigma}^{e(K_1,K_2)}$ takes the form

$$\sigma^{e(K_1,K_2)} = D\left(\boldsymbol{C} : \boldsymbol{\epsilon}^{(K_1,K_2)} - \boldsymbol{\Gamma} T^{(K_1,K_2)}\right) \delta_{K_1,0}\delta_{K_2,0} \tag{12}$$

where $\delta_{i,j}$ is the Kronecker delta. It is obvious that this last expression can be generalized for the modeling of cracks that exist in other cells (as long as it is ensured that the size of the rectangular region is sufficiently large such the far-field at its boundaries is not affected by the cracks existence).

$$\boldsymbol{q}^{(K_1,K_2)} = -\boldsymbol{\kappa}\ \nabla T^{(K_1,K_2)} - \boldsymbol{q}^{e(K_1,K_2)} \tag{13}$$

where

$$\boldsymbol{q}^{e(K_1,K_2)} = -D\boldsymbol{\kappa}\ \nabla T^{(K_1,K_2)}\delta_{K_1,0}\delta_{K_2,0} \tag{14}$$

The governing equations (3)-(4) of the materials within the cell (K_1, K_2) take the form

$$\nabla \cdot \boldsymbol{\sigma}^{(K_1,K_2)} = \mathbf{0} \tag{15}$$

$$\nabla \cdot \boldsymbol{q}^{(K_1,K_2)} = 0 \tag{16}$$

Next, the continuity of displacements $\boldsymbol{u}^{(K_1,K_2)}$ and temperature $T^{(K_1,K_2)}$ between adjacent cells must be imposed. These imply that (the square brackets do not denote quantity jumps)

$$\begin{aligned} &\left[\boldsymbol{u}(d, X_2^{'})\right]^{(K_1,K_2)} - \left[\boldsymbol{u}(-d, X_2^{'})\right]^{(K_1+1,K_2)} = 0, \\ &K_1 = -M_1, ..., M_1 - 1, \qquad K_2 = -M_2, ..., M_2 \end{aligned} \tag{17}$$

$$\begin{aligned} &\left[T(d, X_2^{'})\right]^{(K_1,K_2)} - \left[T(-d, X_2^{'})\right]^{(K_1+1,K_2)} = 0, \\ &K_1 = -M_1, ..., M_1 - 1, \qquad K_2 = -M_2, ..., M_2 \end{aligned} \tag{18}$$

and

$$\begin{aligned} &\left[\boldsymbol{u}(X_1^{'}, h)\right]^{(K_1,K_2)} - \left[\boldsymbol{u}(X_1^{'}, -h)\right]^{(K_1,K_2+1)} = 0, \\ &K_1 = -M_1, ..., M_1, \qquad K_2 = -M_2, ..., M_2 - 1 \end{aligned} \tag{19}$$

$$\begin{aligned} &\left[T(X_1^{'}, h)\right]^{(K_1,K_2)} - \left[T(X_1^{'}, -h)\right]^{(K_1,K_2+1)} = 0, \\ &K_1 = -M_1, ..., M_1, \qquad K_2 = -M_2, ..., M_2 - 1 \end{aligned} \tag{20}$$

Similarly, the continuity of tractions $\boldsymbol{t}^{(K_1,K_2)}$ and the normal components of the heat flux $\boldsymbol{q}^{(K_1,K_2)}$ between adjacent cells are fulfilled by requiring that

$$\begin{aligned} &\left[\boldsymbol{t}(d, X_2^{'})\right]^{(K_1,K_2)} - \left[\boldsymbol{t}(-d, X_2^{'})\right]^{(K_1+1,K_2)} = 0, \\ &K_1 = -M_1, ..., M_1 - 1, \qquad K_2 = -M_2, ..., M_2 \end{aligned} \tag{21}$$

$$K_1 = -M_1, ..., M_1 - 1, \qquad K_2 = -M_2, ..., M_2 \tag{22}$$

and

$$\Big[\boldsymbol{t}(X_1^{'}, h)\Big]^{(K_1,K_2)} - \Big[\boldsymbol{t}(X_1^{'}, -h)\Big]^{(K_1,K_2+1)} = 0,$$
$$K_1 = -M_1, ..., M_1, \qquad K_2 = -M_2, ..., M_2 - 1 \tag{23}$$

$$\Big[q_2(X_1^{'}, h)\Big]^{(K_1,K_2)} - \Big[q_2(X_1^{'}, -h)\Big]^{(K_1,K_2+1)} = 0,$$
$$K_1 = -M_1, ..., M_1, \qquad K_2 = -M_2, ..., M_2 - 1 \tag{24}$$

Finally, the boundary conditions have to be imposed on the boundaries $\pm D$ and $\pm H$ of the rectangle which, as stated before, must be sufficiently far away such that the effect of the crack is negligible. The tractions and the normal components of the heat flux on opposite sufficiently remote sides of this rectangle must be equal. Thus

$$\Big[\sigma_{1j}(d, X_2^{'})\Big]^{(M_1,s)} - \Big[\sigma_{1j}(-d, X_2^{'})\Big]^{(-M_1,s)} = 0, \qquad s = -M_2, ..., M_2 \tag{25}$$

$$\Big[q_1(d, X_2^{'})\Big]^{(M_1,s)} - \Big[q_1(-d, X_2^{'})\Big]^{(-M_1,s)} = 0, \qquad s = -M_2, ..., M_2 \tag{26}$$

and

$$\Big[\sigma_{2j}(x_1^{'}, h)\Big]^{(r,M_2)} - \Big[\sigma_{2j}(X_1^{'}, -h)\Big]^{(r,-M_2)} = 0, \qquad r = -M_1, ..., M_1 \tag{27}$$

$$\Big[q_2(X_1^{'}, h)\Big]^{(r,M_2)} - \Big[q_2(X_1^{'}, -h)\Big]^{(r,-M_2)} = 0, \qquad r = -M_1, ..., M_1 \tag{28}$$

On the other hand, the displacements and temperature at these opposite sides differ. Their differences (jumps) are defined by

$$\boldsymbol{u}^{(M_1,s)}(d, X_2^{'}) - \boldsymbol{u}^{(-M_1,s)}(-d, X_2^{'}) \equiv \boldsymbol{J}_1^u, \qquad s = -M_2, ..., M_2 \tag{29}$$

$$T^{(M_1,s)}(d, X_2^{'}) - T^{(-M_1,s)}(-d, X_2^{'}) \equiv J_1^T, \qquad s = -M_2, ..., M_2 \tag{30}$$

$$\boldsymbol{u}^{(r,M_2)}(X_1^{'},h)-\boldsymbol{u}^{(r,-M_2)}(X_1^{'},-h)\equiv \boldsymbol{J}_2^u, \qquad r=-M_1,...,M_1 \tag{31}$$

$$T^{(r,M_2)}(X_1^{'},h)-T^{(r,-M_2)}(X_1^{'},-h)\equiv J_2^T, \qquad r=-M_1,...,M_1 \tag{32}$$

These jumps are the given by the far-field (which is not affected by the crack existence) as follows

$$J_{1k}^u=2D\bar{\epsilon}_{1k}, \qquad J_{2k}^u=2H\bar{\epsilon}_{2k}, \qquad k=1,2,3 \tag{33}$$

where $\bar{\epsilon}_{1k}$ and $\bar{\epsilon}_{2k}$ are the average (far-field) strain of the unperturbed periodic composite. They can be determined from the micromechanically established macroscopic (average) constitutive law:

$$\bar{\boldsymbol{\sigma}}=\boldsymbol{C}^*:\bar{\boldsymbol{\epsilon}}-\boldsymbol{\Gamma}^*T \tag{34}$$

where $\boldsymbol{C}^*$ and $\boldsymbol{\Gamma}^*$ are the effective stiffness and thermal stress tensors of the periodic (unperturbed) composite which can be determined by HFGMC micromechanical analysis, Aboudi et al. (2013), and $\bar{\boldsymbol{\sigma}}$ are the far-field applied tractions. When the composite is subjected to a heat flux only (i.e., in the absence of a strain loading), the average (far-field) strains $\bar{\boldsymbol{\epsilon}}$ are equal to zero.

Similarly,

$$J_1^T=2D\bar{\tau}_1, \qquad J_2^T=2H\bar{\tau}_2 \tag{35}$$

where $\bar{\tau}_1$ and $\bar{\tau}_2$ are the components of the remote temperature gradient. They can be determined from the micromechanically established macroscopic (average) Fourier law of the composite:

$$\bar{\boldsymbol{q}}=-\boldsymbol{\kappa}^*\bar{\boldsymbol{\tau}} \tag{36}$$

with $\boldsymbol{\kappa}^*$ being the effective thermal conductivity tensor that can be determined from HFGMC analysis, Bednarcyk et al. (2017), and $\bar{\boldsymbol{q}}$ is the far-field applied heat flux.

3.2 Formulation in the transform domain

The next stage in the representative cell method consists of the application of the double discrete Fourier transform. For the displacement vector $\boldsymbol{u}^{(K_1,K_2)}$ (for example) this transform is defined

Peer-reviewed version available at J. Compos. Sci. 2017, 1, , 4; doi:10.3390/jcs1010004

$$\hat{\boldsymbol{u}}(X_1^{'}, X_2^{'}, \phi_r, \phi_s) = \sum_{K_1=-M_1}^{M_1} \sum_{K_2=-M_2}^{M_2} \boldsymbol{u}^{(K_1,K_2)}(X_1^{'}, X_2^{'}) \exp\left[i(K_1\phi_r + K_2\phi_s)\right] \tag{37}$$

where

$$\phi_r = \frac{2\pi r}{2M_1+1}, \qquad r = 0, \pm 1, \pm 2, ..., \pm M_1, \qquad \phi_s = \frac{2\pi s}{2M_2+1}, \qquad s = 0, \pm 1, \pm 2, ..., \pm M_2,$$

The application of this transform to the boundary problem (11)-(32) for the rectangular domain $-D < X_1 < D$, $-H < X_2 < H$, which is divided into $(2M_1+1) \times (2M_2+1)$ cells, converts it to the problem for the single representative cell $-d < X_1^{'} < d$, $-h < X_2^{'} < h$ with respect to the complex valued transforms. The resulting constitutive equations (11)-(14) take the form

$$\hat{\boldsymbol{\sigma}} = \boldsymbol{C} : \hat{\boldsymbol{\epsilon}} - \boldsymbol{\Gamma}\hat{T} - \hat{\boldsymbol{\sigma}}^e \tag{38}$$

$$\hat{\sigma}^e = D\left(\boldsymbol{C} : \hat{\boldsymbol{\epsilon}} - \boldsymbol{\Gamma}\hat{T}\right) \tag{39}$$

$$\hat{\boldsymbol{q}} = -\boldsymbol{\kappa}\, \nabla\hat{T} - \hat{\boldsymbol{q}}^e \tag{40}$$

$$\hat{\boldsymbol{q}}^e = -D\boldsymbol{\kappa}\, \nabla\hat{T} \tag{41}$$

The governing equations (15)-(16) reduce to

$$\nabla \cdot \hat{\boldsymbol{\sigma}} = \boldsymbol{0} \tag{42}$$

$$\nabla \cdot \hat{\boldsymbol{q}} = 0 \tag{43}$$

Next, the continuity conditions (17)-(28) in the transform domain are

$$\hat{\boldsymbol{u}}(d, X_2^{'}) - \exp(-i\phi_r)\hat{\boldsymbol{u}}(-d, X_2^{'}) = 0, \qquad -h \le X_2^{'} \le h \tag{44}$$

$$\hat{T}(d, X_2^{'}) - \exp(-i\phi_r)\hat{T}(-d, X_2^{'}) = 0, \qquad -h \le X_2^{'} \le h \tag{45}$$

$$\hat{\boldsymbol{u}}(X_1^{'}, h) - \exp(-i\phi_s)\hat{\boldsymbol{u}}(X_1^{'}, -h) = 0, \qquad -d \le X_1^{'} \le d \tag{46}$$

Peer-reviewed version available at J. Compos. Sci. 2017, 1, , 4; doi:10.3390/jcs1010004

$$\hat{\boldsymbol{t}}(d, X_2^{'}) - \exp(-i\phi_r)\hat{\boldsymbol{t}}(-d, X_2^{'}), \qquad -h \leq X_2^{'} \leq h \tag{48}$$

$$\hat{q}_1(d, X_2^{'}) - \exp(-i\phi_r)\hat{q}_1(-d, X_2^{'}), \qquad -h \leq X_2^{'} \leq h \tag{49}$$

$$\hat{\boldsymbol{t}}(X_1^{'}, h) - \exp(-i\phi_s)\hat{\boldsymbol{t}}(X_1^{'}, -h), \qquad -d \leq X_1^{'} \leq d \tag{50}$$

$$\hat{q}_2(X_1^{'}, h) - \exp(-i\phi_s)\hat{q}_2(X_1^{'}, -h), \qquad -d \leq X_1^{'} \leq d \tag{51}$$

In all these equations, $r = 0, ..., \pm M_1$; $s = 0, ..., \pm M_2$.

As to the displacements and temperature differences (jumps) that are given by (29)-(32), they appear in the transform domain as follows:

$$\hat{\boldsymbol{u}}(d, X_2^{'}) - \exp(-i\phi_r)\hat{\boldsymbol{u}}(-d, X_2^{'}) + \delta_{0,s}(2M_2 + 1)\boldsymbol{J}_1^u \exp(i\phi_r M_1), \qquad -h \leq X_2^{'} \leq h \tag{52}$$

$$\hat{T}(d, X_2^{'}) - \exp(-i\phi_r)\hat{T}(-d, X_2^{'}) + \delta_{0,s}(2M_2 + 1)J_1^T \exp(i\phi_r M_1), \qquad -h \leq X_2^{'} \leq h \tag{53}$$

$$\hat{\boldsymbol{u}}(X_1^{'}, h) - \exp(-i\phi_s)\hat{\boldsymbol{u}}(X_1^{'}, -h) + \delta_{0,r}(2M_1 + 1)\boldsymbol{J}_2^u \exp(i\phi_s M_2), \qquad -d \leq X_1^{'} \leq d \tag{54}$$

$$\hat{T}(X_1^{'}, h) - \exp(-i\phi_s)\hat{T}(X_1^{'}, -h) + \delta_{0,r}(2M_1 + 1)J_2^T \exp(i\phi_s M_2), \qquad -d \leq X_1^{'} \leq d \tag{55}$$

The set of equations (38)-(55) define a boundary value problem in the transform domain. These equations can be solved by the methods that have been presented in detail in Chapter 11 of Aboudi et al. (2013) for functionally graded materials. Thus, the representative cell domain $-d \leq X_1^{'} \leq d$, $-h \leq X_2^{'} \leq h$ is divided into several rectangular subcells, $\alpha = 1, ..., N_\alpha$, $\beta = 1, ..., N_\beta$, see Fig. 1(c). The transformed displacement vector and temperature are expanded into second-order polynomials, and the equilibrium and heat equations, interfacial and boundary conditions are imposed in the average (integral) sense. This results in a system of algebraic equations the solution of which provides the transformed thermal and mechanical fields. The actual fields at any point within the cells (K_1, K_2) of the considered rectangular region $-D \leq X_1 \leq D$,

Preprints (www.preprints.org) | NOT PEER-REVIEWED | Posted: 25 May 2017 doi:10.20944/preprints201705.0182.v1

Peer-reviewed version available at J. Compos. Sci. 2017, 1, , 4; doi:10.3390/jcs1010004

displacement vector (for example) is given by:

$$\boldsymbol{u}^{(K_1,K_2)}(X_1^{'},X_2^{'})=\frac{1}{(2M_1+1)(2M_2+1)}\sum_{r=-M_1}^{M_1}\sum_{s=-M_2}^{M_2}\hat{\boldsymbol{u}}(X_1^{'},X_2^{'},\phi_r,\phi_s)\exp\left[-i(K_1\phi_r+K_2\phi_s)\right] \quad (56)$$

In the application of this solution, the eigenfield vectors $\hat{\boldsymbol{\sigma}}^e$ and $\hat{\boldsymbol{q}}^e$ to be employed in Eqs. (38) and (40) are not known. Hence an iterative solution has to be employed as follows.

1. Start by assuming that $\hat{\boldsymbol{\sigma}}^e=\mathbf{0}$ and $\hat{\boldsymbol{q}}^e=\mathbf{0}$ and solve the above equations in the transform domain.

2. Apply the inverse transform formula to compute the thermal and stress fields. The field variables in the actual space can be employed to compute the current eigenfields $\boldsymbol{\sigma}^{e(K_1,K_2)}$ and $\boldsymbol{q}^{e(K_1,K_2)}$.

3. Compute the transforms of $\boldsymbol{\sigma}^{e(K_1,K_2)}$ and $\boldsymbol{q}^{e(K_1,K_2)}$, (39) and (41), to be employed in Eqs. (38) and (40).

4. Solve again the equations in the transform domain.

This procedure should be continued until a convergence to a desired degree of accuracy is achieved.

The computational efficiency of the present approach can be illustrated by considering the analysis of the cracked fiber-reinforced material with the fibers forming a hexagonal array, that will be discussed in the following. This composite region has been divided into 11×11 cells (i.e., $M_2=M_3=5$). The representative cell has been divided in the framework of the higher-order theory into $N_\alpha=100$ and $N_\beta=56$ subcells (which has been found to provide accurate results). The higher-order analysis requires the solution of 16 unknowns in each subcell (i.e. 32 unknowns in the complex transform domain). Hence, this discretization requires for each combination of ϕ_r, ϕ_s the solution of a sparse system of 179,200 algebraic equations. A direct numerical solution (e.g., by a finite element procedure) with the same number of degrees of freedom would require solving a system of $11\times 11\times 16\times 100\times 56\approx 10\times 10^6$ equations which is very large. Another significant advantage of the present analysis over a direct computational approach stems from the fact that by increasing the size of the rectangular region $-D\le X_1\le D$, $-H\le X_2\le H$ (in order to further diminish the crack effect) within which the computations in the transform domain are carried out (i.e., by increasing M_1 and M_2) the number of algebraic equations (179,200 in the

increases with the increase of M_1 and M_2.

4. Verifications

In Tarn and Wang (1993), an exact solution for the temperature and thermal stresses fields are given for a crack of length $2a$ embedded within an infinite homogeneous anisotropic material. The material is subjected to a remote heat flux $\bar{\boldsymbol{q}}$, and the crack is traction-free and insulated such that its surface heat flux is equal to zero. With the effective heat conductivity, stiffness, and thermal stress tensors, $\boldsymbol{\kappa}^*$, $\boldsymbol{C}^*$ and $\boldsymbol{\Gamma}^*$ that characterize a considered homogenized anisotropic material, the solution of Tarn and Wang (1993) can be implemented to verify the field variation as predicted by the present analysis. The exact expressions for the temperature and heat flux are given by

$$T = 2Re(g'(z_t)) \tag{57}$$

$$q_1 = -2Re\left(\kappa_{11}^* g''(z_t)\right), \qquad q_2 = -2Re\left(\mu_t \kappa_{22}^* g''(z_t)\right) \tag{58}$$

where

$$g(z_t) = -\frac{i\bar{q}_2 a^2}{4\sqrt{\kappa_{11}^*\kappa_{22}^*}}\left[ln\left(z_t + \sqrt{z_t^2 - a^2}\right) + \frac{1}{a^2}\left(z_t^2 - z_t\sqrt{z_t^2 - a^2}\right)\right] \tag{59}$$

and $z_t = X_1 + \mu_t X_2$ with $\mu_t = i\sqrt{\kappa_{11}^*/\kappa_{22}^*}$.

In addition, the thermal stresses in the cracked material can be determined from the following expression

$$\sigma_{1k} = 2Re\left\{\frac{2}{a(\zeta_k - \zeta_k^{-1})}\left[\boldsymbol{Lh}\right]_k + \frac{i\bar{q}_2 a^2}{4\sqrt{\kappa_{11}^*\kappa_{22}^*}}\right\}, \qquad k = 1, 2, 3 \tag{60}$$

In these equations, $\zeta_k = (z_k + \sqrt{z_k^2 - a^2})/a$, $z_k = X_1\mu_k X_2$ and μ_k are the three roots with the positive imaginary part of a cubic equation that is given together with $\boldsymbol{L}$ and $\boldsymbol{h}$ in Tarn and Wang (1993).

Consider a unidirectional fiber-reinforced composites that consists of carbon T300 fibers reinforcing an epoxy matrix. The volume fraction of the reinforcing fibers is $v_f = 0.5$. The properties

predicted by the HFGMC micromechanical model, are given in Table 1. Let the axial direction of this homogenized composite be oriented in the 1-direction and a crack of length 2a/(2d) = 1 is introduced along this direction, see inset in Fig. 2. The homogenized composite is subjected to a remote heat flux $\bar{q}_2$ = -1 W/m^2 in the 2-direction. Figure 2 shows a comparison between the temperature, heat flux and the induced shear stress along the crack line as predicted by the exact solution of Tarn and Wang (1993) and the present approach. Very good agreement can be observed. It should be noted that only shear stress σ_{12} exists along the crack line, whereas $\sigma_{22} = 0$ along this line. This is in agreement with the result of Sih (1962) who showed that in a cracked isotropic material that is subjected to a remote heat flux, only Mode II deformation exists.

Next, let the axial direction of this homogenized transversely isotropic composite be oriented in the out-of-the plane 3-direction, and a crack of length 2a is introduced along the 1-direction, see inset in Fig. 3. In the present situation the plane X_1-X_2 is a plane of isotropy. In this case, the solution of Tarn and Wang (1993) is not applicable since out of the three roots μ_k, $k = 1, 2, 3$, two of them coincide, and in addition, these two coincide with μ_t (i.e., $\mu_1 = \mu_2 = \mu_t = 1$). It is important however to verify this situation because in the analysis of the cracked (unhomogenized) fiber-reinforced composites and porous materials that will be considered in the next section, the axes of symmetry are oriented in the out-of-plane 3-direction. For this case it is however possible to verify our solution approach by utilizing the exact solution of Koizumi et al. (1979) for a crack embedded in isotropic material that is subjected to a remote heat flux.

The closed-form solution of Koizumi et al. (1979) for the temperature is given by

$$T = -\frac{\bar{q}_2}{\kappa} Re\left\{ i\left[z - \sqrt{z^2 - a^2} \right] \right\} - \frac{\bar{q}_2}{\kappa} X_2 \tag{61}$$

where $z = X_1 + iX_2$ and κ is the heat conduction. The heat flux components can be readily determined from this relation:

$$q_1 = \bar{q}_2 Re\left\{ i\left[1 - \frac{z}{\sqrt{z^2 - a^2}} \right] \right\}, \qquad q_2 = -\bar{q}_2 Re\left\{ 1 - \frac{z}{\sqrt{z^2 - a^2}} \right\} + \bar{q}_2 \tag{62}$$

The induced thermal stresses are determined from the two complex potentials $\varphi(z)$ and $\psi(z)$ as follows.

$$\sigma_{11} + \sigma_{22} = 4Re\left[\varphi'(z)\right], \qquad \sigma_{22} - \sigma_{11} + 2i\sigma_{12} = 2\left[\bar{z}\varphi''(z) + \psi'(z)\right] \tag{63}$$

$$\varphi(z) = \frac{ia^2(1+\nu)\alpha G\bar{q}_2}{4\kappa(1-\nu)} ln \frac{z+\sqrt{z^2-a^2}}{2a} \tag{64}$$

$$\psi(z) = -\varphi(z) - \frac{ia^4(1+\nu)\alpha G\bar{q}_2}{4\kappa(1-\nu)} \frac{1}{\sqrt{z^2-a^2}} \frac{1}{z+\sqrt{z^2-a^2}} \tag{65}$$

where G, ν and α are the shear modulus, Poisson's ratio and coefficient of thermal expansion of the isotropic material, respectively. The constants κ, G, ν and α can be readily determined from the established effective conductivity, stiffness and thermal tensors of the considered composite.

Here too, let the homogenized composite be subjected to a remote heat flux $\bar{q}_2$ = -1 W/m^2 in the 2-direction. In figure 3, comparisons between this exact solution and the present one for the undirectional carbon/epoxy composite whose axis of symmetry is oriented in the out-of-plane X_3-direction with a transverse crack are shown. Very good agreements between the two solutions for the temperature, heat flux and the induced shear stresses along the crack line can be well observed.

5. Applications

In the present section, applications are given for the prediction of the temperature, field, heat flux and induced thermal stresses in a cracked fiber-reinforced polymer matrix composite, porous ceramic material and periodically layered ceramic composite under remote heat flow. In all these cases, the actual effects of the microstructure of the composite are accounted to (i.e., not homogenized). The chosen number of cells which were found to ensure sufficient remoteness from the crack effects are $M_1 = M_2 = 5$

5.1 A cracked fiber-reinforced polymer matrix composite subjected to a remote heat flux

Consider a carbon/epoxy fiber-reinforced composite in which the carbon fibers are oriented in the 3-direction and arranged in a hexagonal array. It is assumed that a transverse crack which connects two adjacent fibers exists, see inset in Fig. 4. The length of the crack is 2a/(2d) =

fiber volume ratio is $v_f = 0.5$. The composite is subjected to a remote normal heat flux $\bar{q}_2$ = -1 W/m^2.

Figure 4 shows the variation along the crack line of the temperature T, normal heat flux q_2 and the induced thermal shear stress σ_{12}. The effect of the composite microstructure is clearly observed by the variations of the various field variables. These field variations can be compared with the corresponding one that have been shown in Fig. 3 where the carbon/epoxy composite was homogenized, as a result of which the microstructure effects were ignored. In the latter homogenized case, for example, the magnitude of the temperature, concentrated at the crack surface, was about 1.4 K, whereas in the actual situation that is shown in Fig. 4 it is about 0.9 K.

In Fig. 5(a), 5(b) and 5(c) the full field distribution of the temperature, normal heat flux and the induced normal thermal stress σ_{22} are shown in the region $-5 \leq X_1/(2d) \leq 5$, $-3 \leq X_2/(2h) \leq 3$ are shown. It can be observed from Fig. 5(a) that the temperature varies between $\pm$7 K whereas the full temperature field in the homogenized case (not shown) exhibits a variation between $\pm$14 K, indicating here too the importance of accounting the microstructure effects. Figure 5(b) shows the effect of the crack existence on the heat flux with its concentration near its tip. The full field distribution of the shear stress σ_{12} is not shown because the most interesting effects exist near the crack tip which has been already shown in Fig. 4. The distribution of the normal thermal stress σ_{22} that is shown in Fig. 5(c) indicates that in the entire vicinity of the crack line this stress is very small (zero along it), and it exhibits an anti-symmetric behavior with respect to this line.

5.2 A cracked porous ceramic material subjected to a remote heat flux

In the next application, a cracked porous alumina in which the porosities are distributed such that they form a hexagonal array is considered, see inset in Fig. 6. The porous alumina is subjected to a remote normal heat flux $\bar{q}_2$ = -1 W/m^2. The properties of the alumina (Al_2O_3) are given in Table 1, and the amount of porosity is 0.25. For this uncracked porous material the HFGMC micromechanical model predicts the following values of the effective thermal conductivities (that are needed in Eq. (36): $\kappa^*_{11} = \kappa^*_{22} = 20.76$ W/(mK). It is assumed that a crack which connects

The variations along the crack line of the temperature, normal heat flux component q_2 and induced shear stress σ_{12} are shown in Fig. 6. The effect of the porous material microstructure is well exhibited, and the values of the temperature along this line are extremely low. The full distributions of the temperature, normal heat flux and the induced shear normal stresses are shown in the region in Fig. 7(a), (b), (c) and (d), respectively. Here too, the temperature is relatively quit low as compared to the resulting temperature in the fiber-reinforced composite. The thermal shear stress σ_{12} is antisymmetric with respect to the X_2-axis, whereas the normal thermal stress σ_{22} is antisymmetric with respect to the crack line (X_1-axis). It is obvious that a homogenization of the thermal and induced stress fields of the porous material will result in the loss of all these details.

5.3 A cracked periodically layered ceramic composite subjected to a remote heat flux

As a final application of the proposed approach, consider a periodically layered ceramic composite that consists of alumina and zirconia layers of equal widths. The properties of these materials are given in Table 1. A transverse crack whose length 2a/(2d)=0.5 is located in the more compliant zirconia layer, see inset to Fig. 8. This layered composite is subjected a remote normal heat flux $\bar{q}_2$ = -1 W/m^2. For the uncracked layered composite, the HFGMC model predicts the effective axial and transverse thermal conductivities: κ^*_{11}=5 W/(mK), κ^*_{22}=18.9 W/(mK).

In Fig. 8, the variations along the crack line of the temperature, normal heat flux component q_2 and the induced shear stress σ_{12} are shown The temperature along the crack surface is quite small and it is negligibly small along its line in the other layers. The high values of the normal heat flux and shear stress in the vicinity of the crack tip are well observed (theoretically singular at the crack tip)

The full shear and normal stress fields that developed in the layered composite are shown in Fig. 9 in the region $-1.5 \leq X_1/(2d) \leq 1.5$, $-1.5 \leq X_2/(2h) \leq 1.5$. The magnitude of the normal stress is seen to be appreciably higher that the shear stress.

A multiscale analysis is offered for the determination of the thermal and mechanical fields in cracked composites that are subjected to heat flow. This analysis has been verified by comparison with exact solutions for cracked isotopic and anisotropic thermoelastic materials (the solution of which is far more complicated than the former). Applications are given for three types of cracked composites, subjected to heat flow. The derived formulation however is general enough and allows the application of remote combined thermomechanical loading.

As discussed, the present method has certain advantages over a direct numerical approach. This stems from the fact that the applied boundary conditions (e.g. the applied heat flux) must be located at a sufficiently remote distance from the localized effects (e.g. a crack). As a result, the number of the resulting equations when a direct numerical procedure is adopted might be extremely large. In the present method however, just one discretized cell in the transform domain need to be considered. Increasing the remoteness of the applied boundary conditions does not affect the discretized cell analysis.

Applications of the present analysis have been presented for composites that consist of a single crack. It is however possible to apply it on composites with multiple cracks, see Baoxing and Xiangzhou (1994) for example. The present formulation have been illustrated for a single crack which forms a simple example of localized damage. It is however possible to consider other types of localized damage in composites such as cavities, soft and stiff inclusions, see Aboudi and Ryvkin (2012). In addition, the modeling of the interaction between two types of damage in composites that are subjected heat flow (e.g., interaction between a crack and cavity) is possible. The results in the present article were confined to the application of remote heat flux, the method can be employed however to obtain the thermomechanical field distributions in damaged composites that are subjected to combined mechanical and heat flow.

4 and 5, respectively). In column 3, the effective properties of carbon/epoxy composite ($v_f = 0.5$) are presented. Here, E_A, E_T, ν_A, ν_T, G_A, α_A, α_T, κ_A and κ_T denote the axial and transverse Young's moduli, axial and transverse Poisson's ratios, axial and transverse coefficients of thermal expansion, axial and transverse conductivities, respectively.

Property	Carbon T300	Epoxy	Homogenized carbon/epoxy v_f= 0.5	Alumina Al_2O_3	Zirconia ZrO_2
E_A(GPa)	220	3.45	111.9	393	207
E_T(GPa)	22	3.45	8.49	393	207
ν_A	0.3	0.35	0.32	0.27	0.32
ν_T	0.35	0.35	0.39	0.27	0.32
G_A(GPa)	22	1.28	3.16	154.7	78.4
$\alpha_A(10^{-6}K^{-1})$	-1.3	54	-0.42	8.4	11
$\alpha_T(10^{-6}K^{-1})$	7	54	37.1	8.4	11
κ_A(W/(mK))	20.5	0.18	10.35	35	2.7
κ_T(W/(mK))	1.46	0.18	0.39	35	2.7

Aboudi, J. and Ryvkin, M. (2012). The effect of localized damage on the behavior of composites with periodic microstructure. Int. J. Engng. Sci. 52, 41-55.

Aboudi, J., Arnold, S.M. and Bednarcyk, B.A. 2013. *Micromechanics of Composite Materials: A Generalized Multiscale Analysis Approach*. Elsevier, Oxford, UK.

Baoxing, C. and Xiangzhou, Z., 1994. Orthotropic thermoelasticity problem of symmetrical heat flow disturbed by three coplaner cracks. Int. J. Fracture 67, 301-314.

Bednarcyk, B.A., Aboudi, J. and Arnold, S.M., 2017. Micromechanics of composite materials governed by vector constitutive laws. Int. J. Solids Struct. 110-111, 137-151.

Duflot, M., 2007. The extended finite element method in thermoelastic fracture mechanics. Int. J. Num. Meth. Eng. 74, 827-847.

Hwu, C., 1990. Thermal stresses in an anisotropic plate disturbed by an insulated elliptic hole or crack. J. Appl. Mech. 57, 916-922.

Hwu, C., 1992. Thermoelastic interface crack problems in dissimial anisotropic materials. Int. J. Solids Struct. 16, 2077-2090.

Hwu, C., 2010. Anisotropic Elastic Plates. Springer, New York.

Itou, S., 2000. Thermal stress intensity factors in an infinite orthotropic layer with a crack. Int. J. Fract. 103, 279-291.

Koizumi, T., Takakuda, K., Shibuya, T. and Nishizawa, T., 1979. An infinite plate with a flaw and subjected to uniform heat flow. J. Thermal Streses 2, 341-351.

Kuo, A-Y, 1990. Effects of crack surface heat conductance on stress intensity factors. J. Appl. Mech. 57, 354-358.

Ryvkin, M. and Aboudi, J., 2012. Stress distribution due to cracking in periodically layered composites. Eng. Fract. Mech. 93, 225-238.

tative cell method. Comp. Mech. 20, 145-149.

Sih. G.C., 1962. On the singular character of thermal stresses near a crack tip. J. Appl. Mech. 29, 587-589.

Sturla, F.A. and Barber, J.R., 1988. Thermal stresses due to a plane crack in general anisotropic material. J. Appl. Mech. 55, 372-376.

Tarn, J-Q and Wang, Y-M, 1993. Thermal stresses in anisotropic bodies with a hole or rigid inclusion. J. Thermal Streses 16, 455-471.

Ting, T.C.T. and Yan, G., 1992. The $r^{-1/2}$(ln r) singularity at interface cracks in anisotropic bimaterials due to heat flow. J. Thermal Streses 15, 85-99.

Tsai, Y.M., 1984. Orthotropic thermoelastic problem of uniform heat flow disturbed by a central crack. J. Composite Mat. 18, 122-131.

Ursescu, A. and Dascalu, C., 2006. Thermally conductive elliptic inhomogeneities in 2D anisotropic solids. Arch. Appl. Mech. 75, 541-551.

Wu, C.H., 1984. Plane anisotropic thermoelasticity. J. Appl. Mech. 51, 724-726.

Zhong, X-C, Wu, B., 2012. Thermoelastic analysis for an opening crack in an orthotropic material. Int. J. Fract. 173, 49-55.

Fig. 1: (a) A crack of length $2a$ embedded in a composite material. (b) A rectangular domain $2D \times 2H$ of the composite is divided into repeating cells. These cells are labeled by (K_1, K_2) with $-M_1 \leq K_1 \leq M_1$ and $-M_2 \leq K_2 \leq M_2$, and the size of every one of which is $2d \times 2h$ (the figure is shown for $M_1 = M_2 = 2$). (c) A representative cell in which local coordinates $(X_1^{'}, X_2^{'})$ are introduced whose origin is located at the center. The cell is divided into $N_\alpha \times N_\beta$ subcells.

Fig. 2: Homogenized carbon/epoxy unidirectional transversely isotropic composite with a transverse crack, subjected to a remote normal heat flux of $\bar{q}_2$ =-1 W/m^2. The axial direction of the homogenized composite is oriented in the 1-direction, Comparison between the exact solution of Tarn and Wang (1993) and the present one for the temperature, normal heat flux and shear stress along the crack line.

Fig. 3: Homogenized carbon/epoxy unidirectional transversely isotropic composite with a transverse crack, subjected to a remote normal heat flux of $\bar{q}_2$ =-1 W/m^2. The axial direction of the homogenized composite is oriented in the out-of-plane 3-direction, Comparison between the exact solution of Koizumi et al. (1979) and the present one for the temperature, normal heat flux and shear stress along the crack line.

Fig. 4: The variations along the crack line of the temperature, normal component of the heat flux and induced shear stress that develop in the carbon/epoxy fiber-reinforced composite, subjected to a remote normal heat flux of $\bar{q}_2$ =-1 W/m^2.

Fig. 5: Field distributions in the region $-5 \leq X_1/(2d) \leq 5$, $-3 \leq X_2/(2h) \leq 3$ of the cracked carbon/epoxy fiber-reinforced composite, (a) Temperature T (K) distribution, (b) normal component of the heat flux (W/m^2), (c) normal stress σ_{22} (MPa).

Fig. 6: The variations along the crack line of the temperature, normal component of the heat flux and shear stress that develop in the porous alumina material, subjected to a remote normal heat flux of $\bar{q}_2$ =-1 W/m^2.

porous alumina material. (a) Temperature T (K) distribution, (b) normal component of the heat flux q_2 (W/m^2), (c) shear stress σ_{12} (MPa), (d) normal stress σ_{22} (MPa).

Fig. 8: The variations along the crack line of the temperature, normal component of the heat flux and shear stress that develop in the periodically layered alumina/zirconia, subjected to a remote normal heat flux of $\bar{q}_2$ =-1 W/m^2.

Fig. 9: Field distributions in the region $-1.5 \leq X_1/(2d) \leq 1.5$, $-1.5 \leq X_2/(2h) \leq 1.5$ of the cracked layered ceramic composite. (a) shear stress σ_{12} (MPa), (b) normal stress σ_{22} (MPa).

Preprints (www.preprints.org) | NOT PEER-REVIEWED | Posted: 25 May 2017 doi:10.20944/preprints201705.0182.v1

Peer-reviewed version available at J. Compos. Sci. 2017, 1, , 4; doi:10.3390/jcs1010004

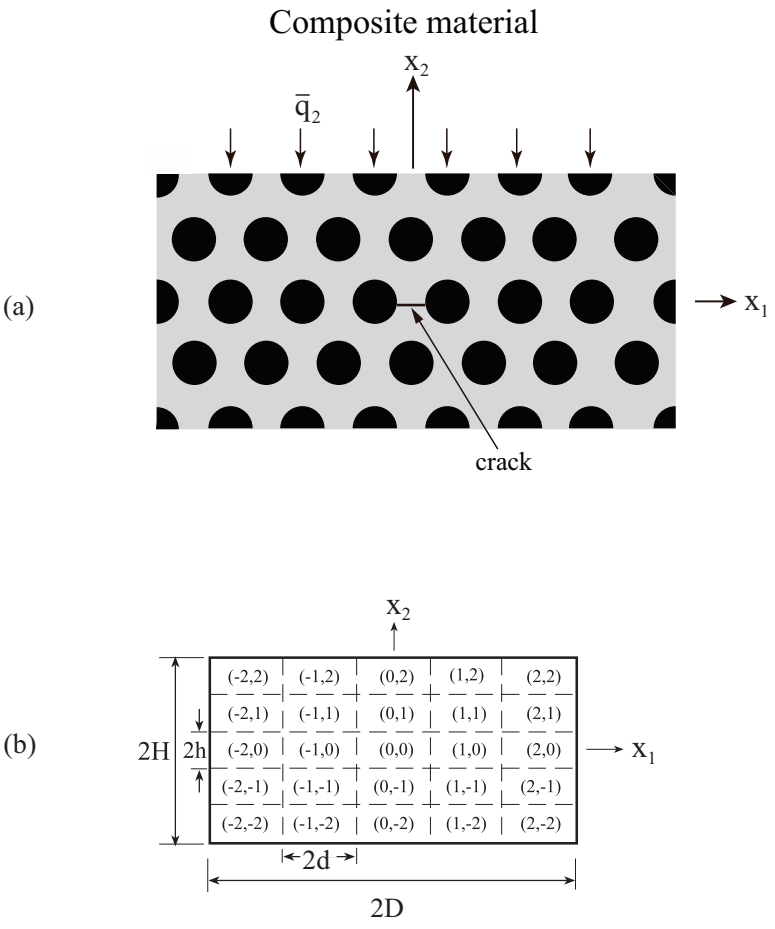

Fig.1

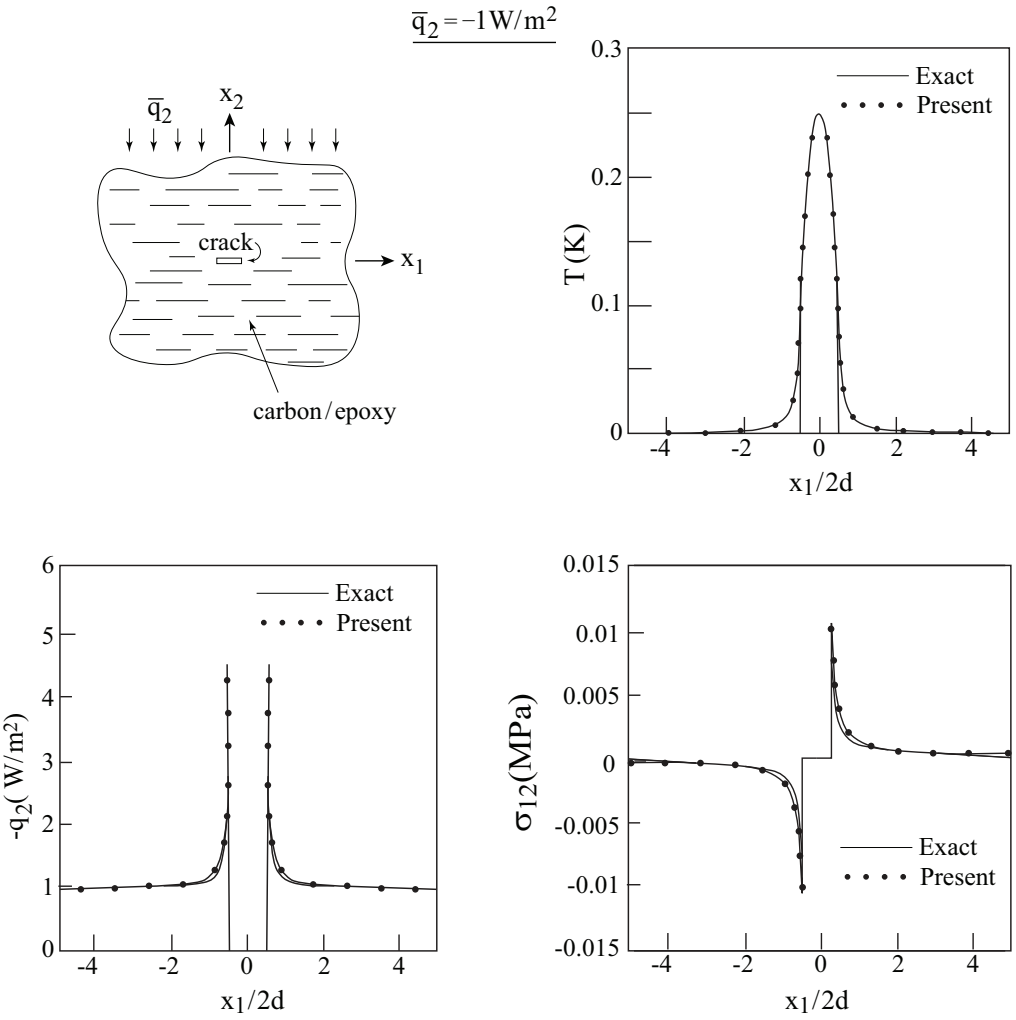

Fig.2

Preprints (www.preprints.org) | NOT PEER-REVIEWED | Posted: 25 May 2017 doi:10.20944/preprints201705.0182.v1

Peer-reviewed version available at J. Compos. Sci. 2017, 1, , 4; doi:10.3390/jcs1010004

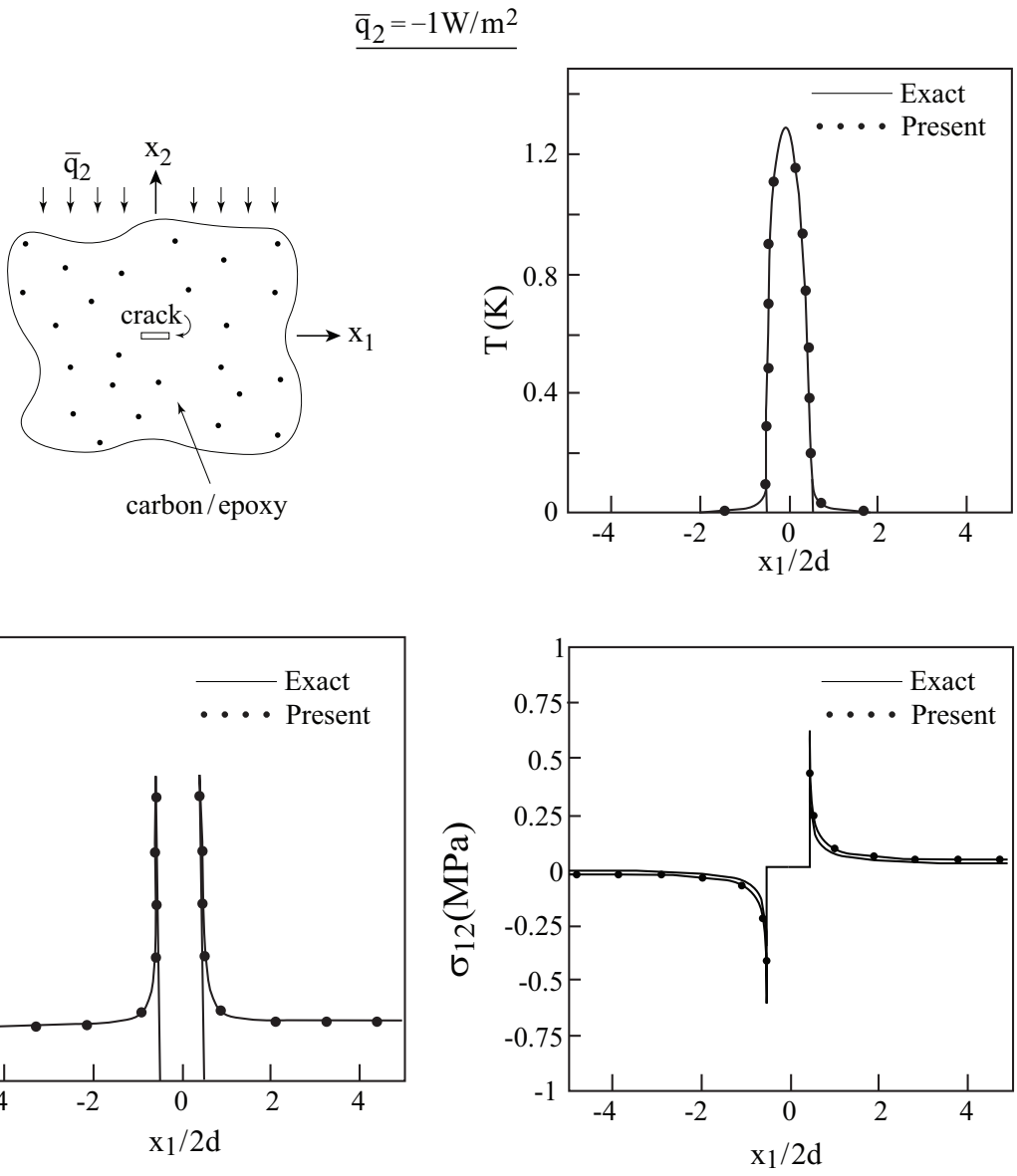

Fig.3

Preprints (www.preprints.org) | NOT PEER-REVIEWED | Posted: 25 May 2017 doi:10.20944/preprints201705.0182.v1

Peer-reviewed version available at J. Compos. Sci. 2017, 1, , 4; doi:10.3390/jcs1010004

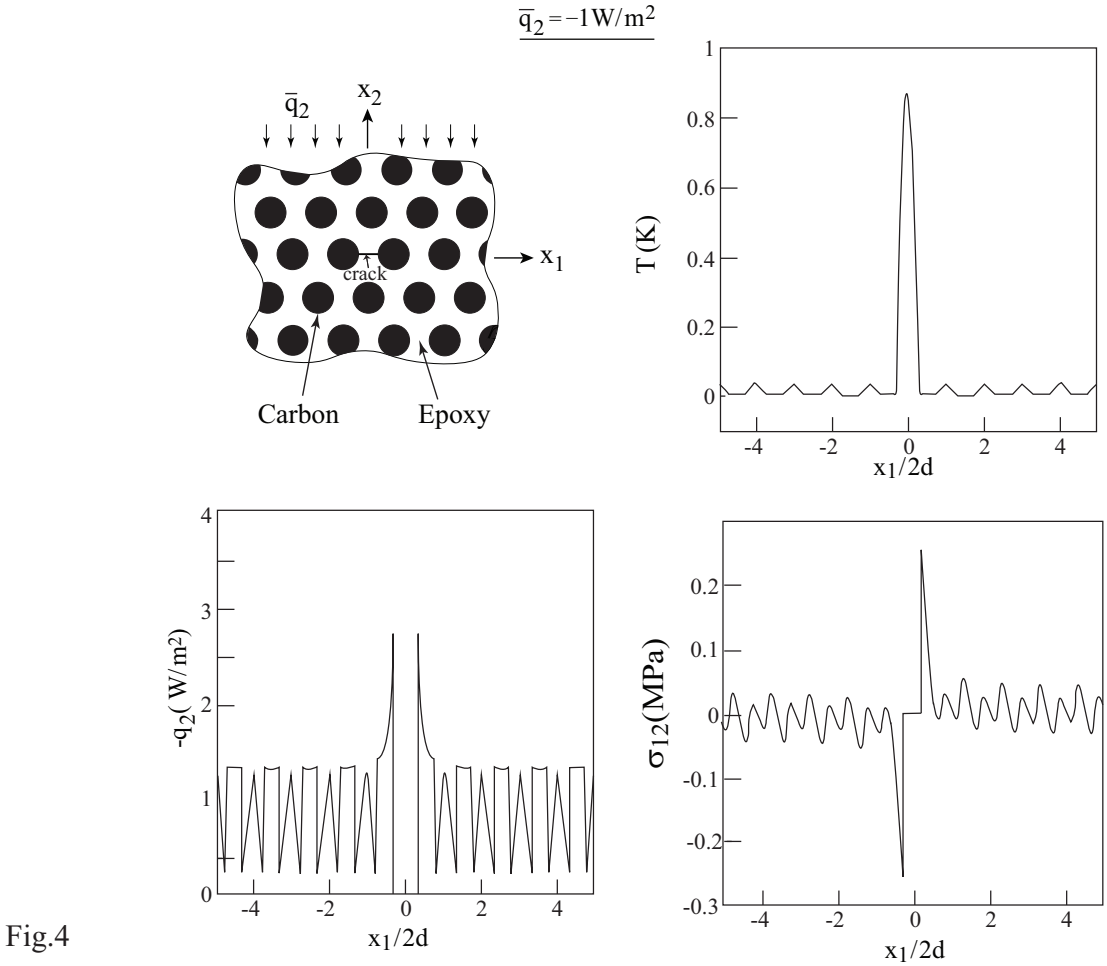

Fig.4

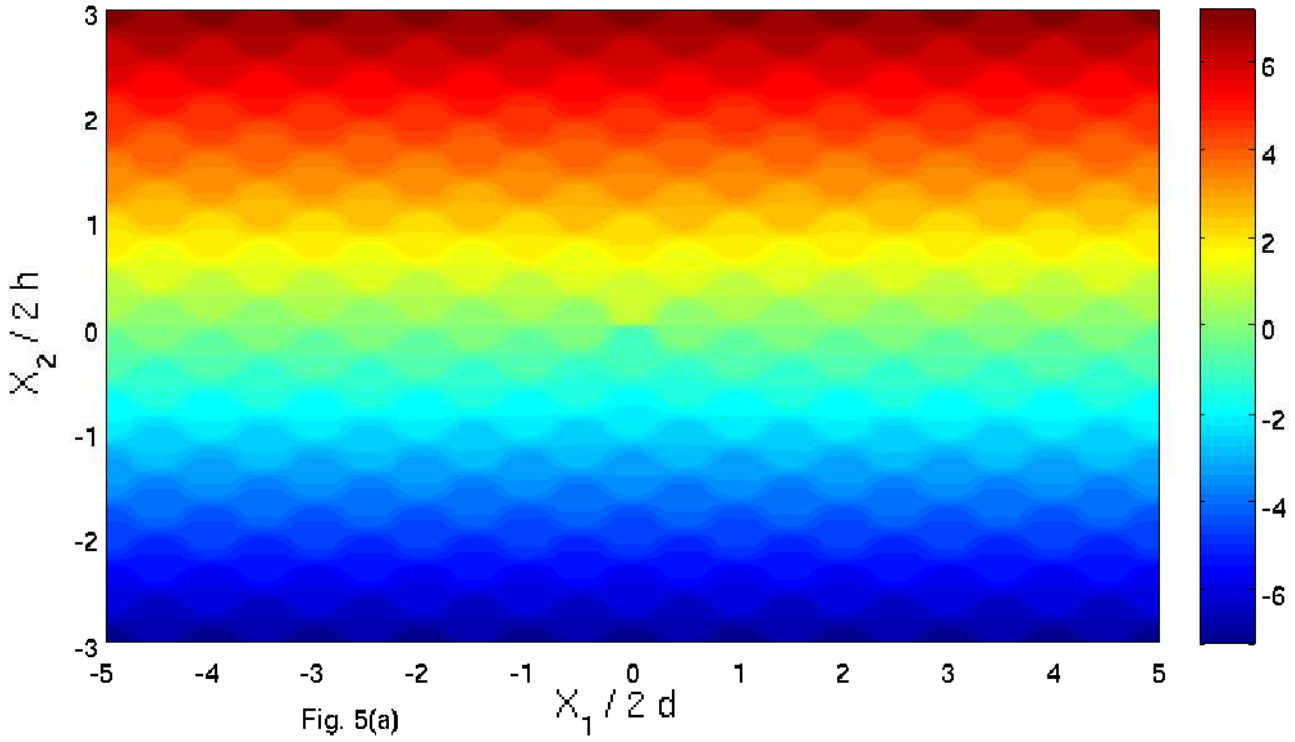

Fig. 5(a)

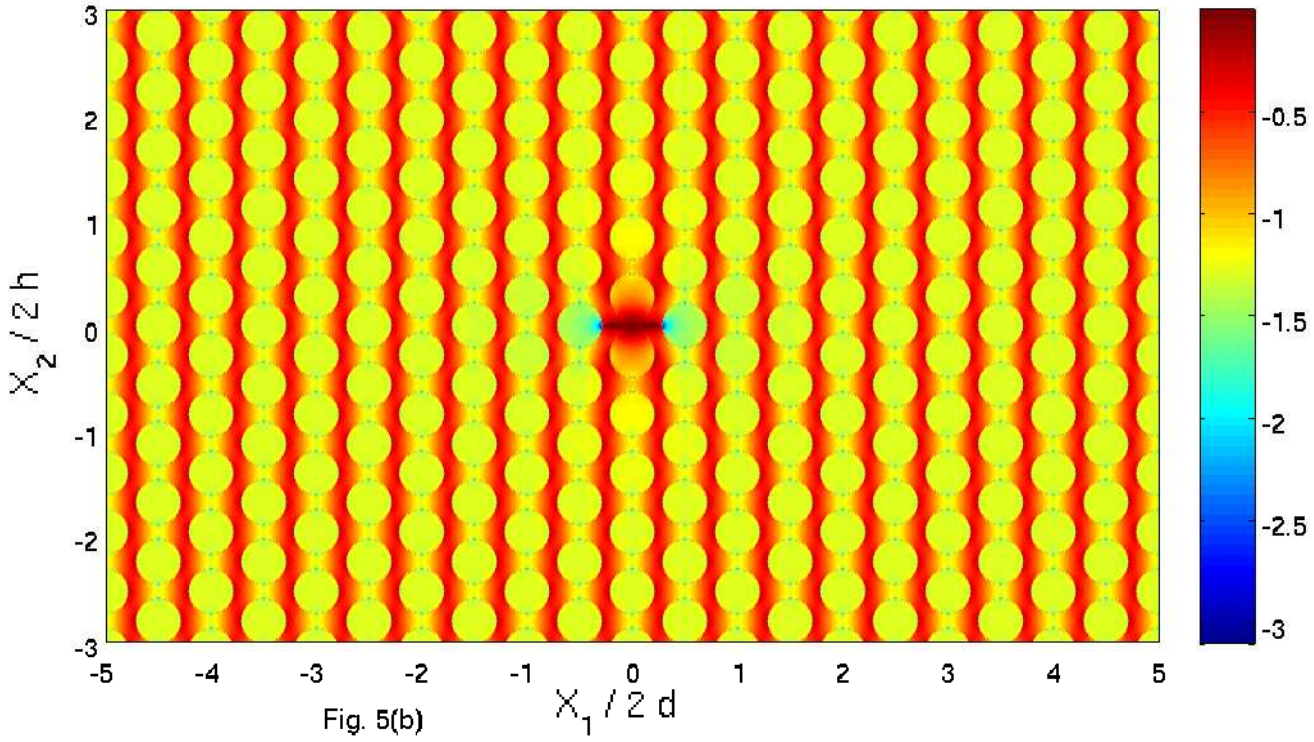

Fig. 5(b)

Preprints (www.preprints.org) | NOT PEER-REVIEWED | Posted: 25 May 2017 doi:10.20944/preprints201705.0182.v1

Peer-reviewed version available at *J. Compos. Sci.* **2017**, *1*, , 4; doi:10.3390/jcs1010004

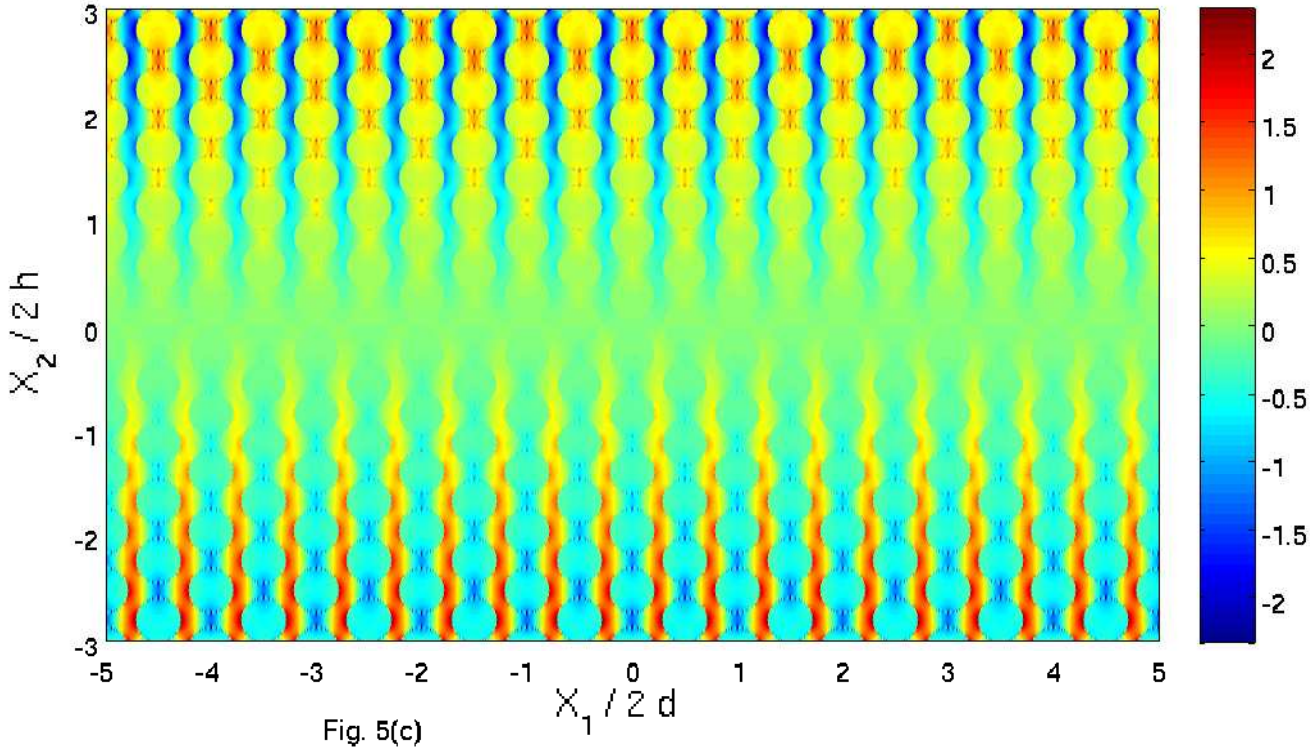

Fig. 5(c)

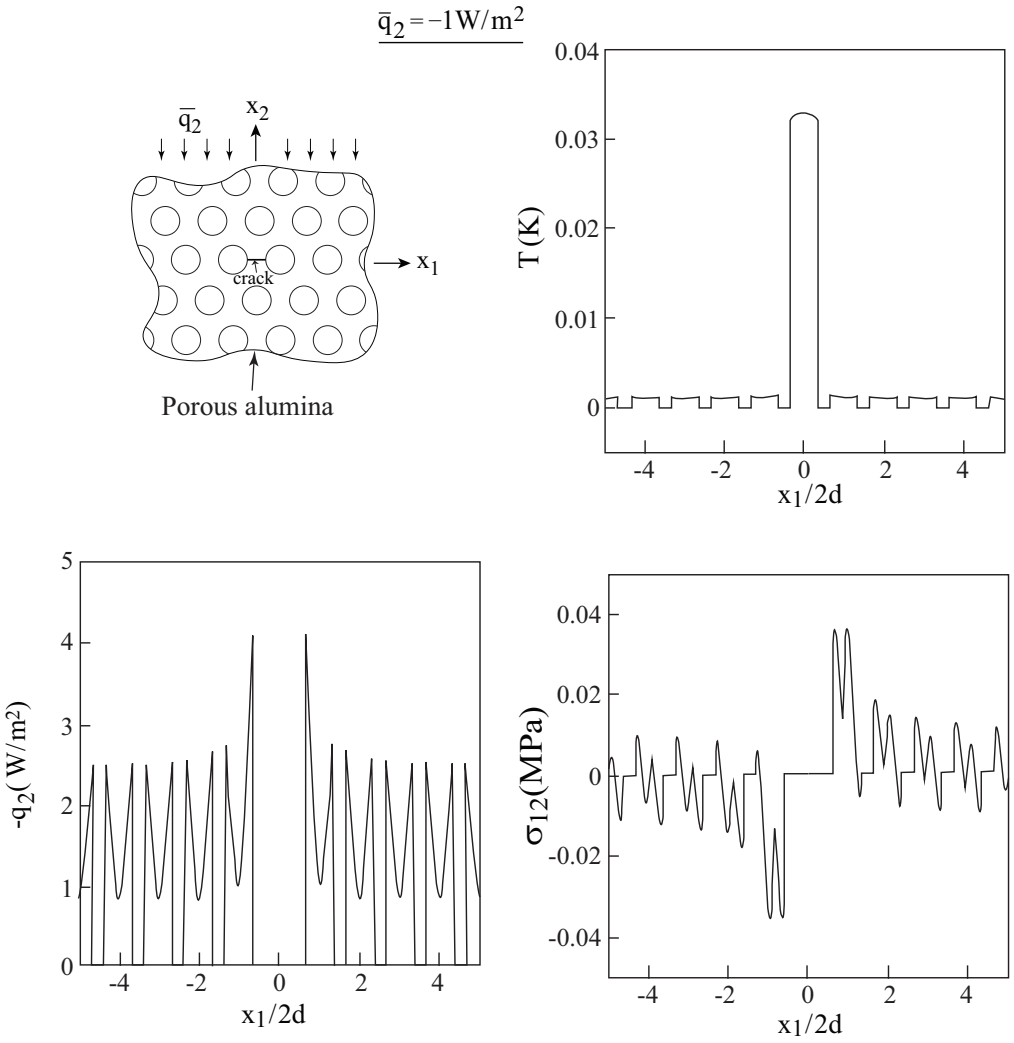

Fig.6

Preprints (www.preprints.org) | NOT PEER-REVIEWED | Posted: 25 May 2017 doi:10.20944/preprints201705.0182.v1

Peer-reviewed version available at *J. Compos. Sci.* **2017**, *1*, , 4; doi:10.3390/jcs1010004

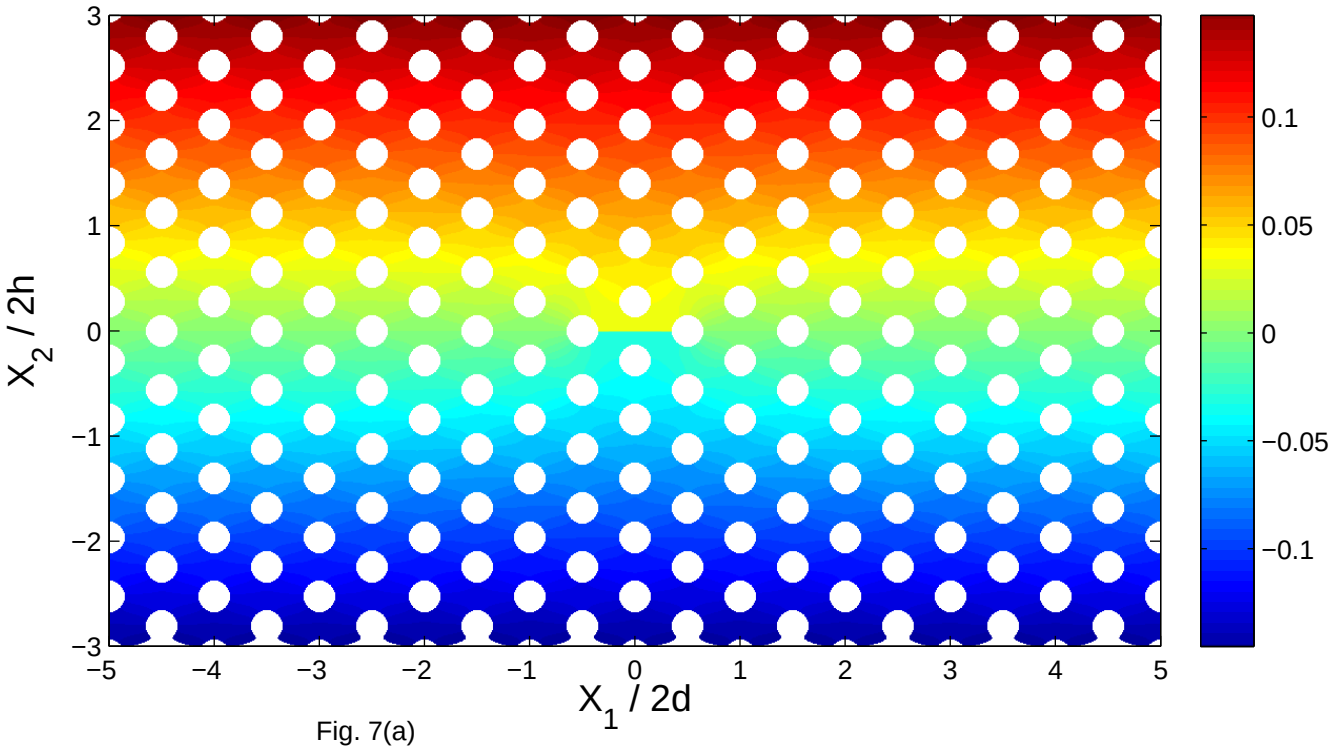

Fig. 7(a)

Preprints (www.preprints.org) | NOT PEER-REVIEWED | Posted: 25 May 2017 doi:10.20944/preprints201705.0182.v1

Peer-reviewed version available at *J. Compos. Sci.* **2017**, *1*, , 4; doi:10.3390/jcs1010004

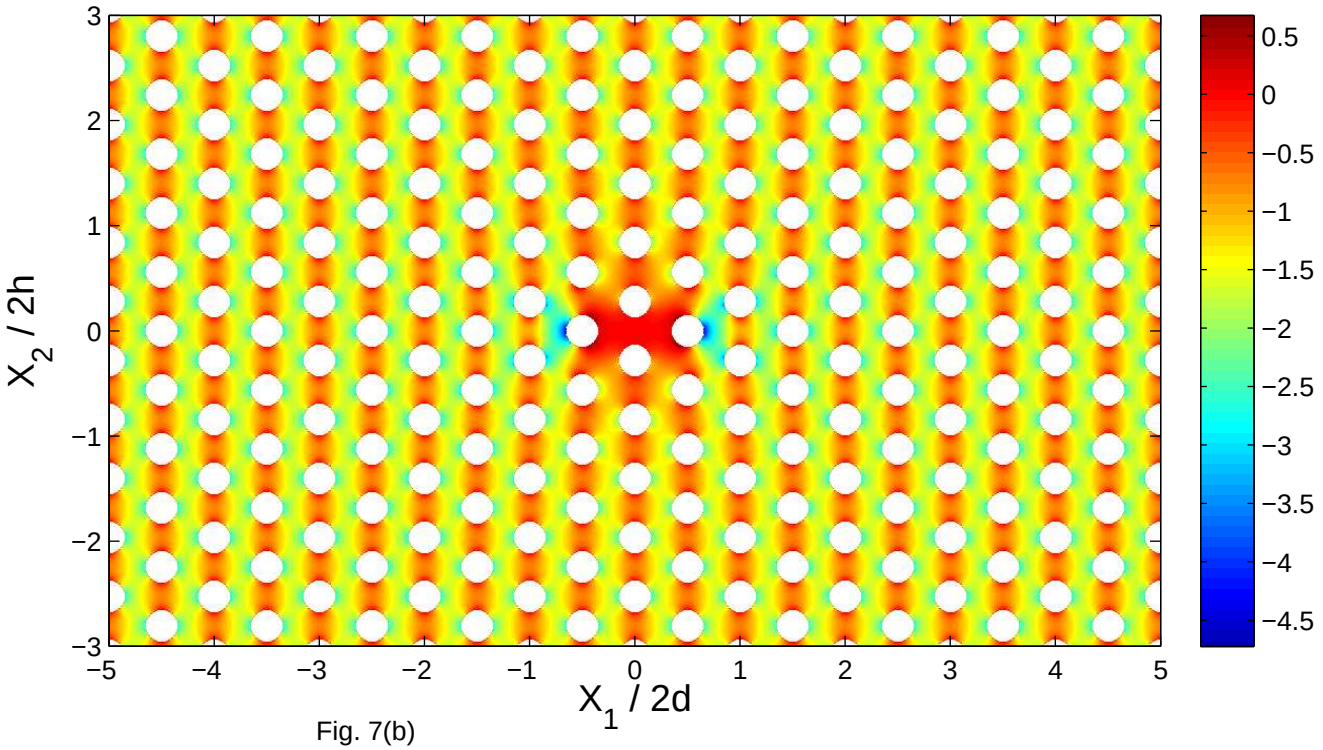

Fig. 7(b)

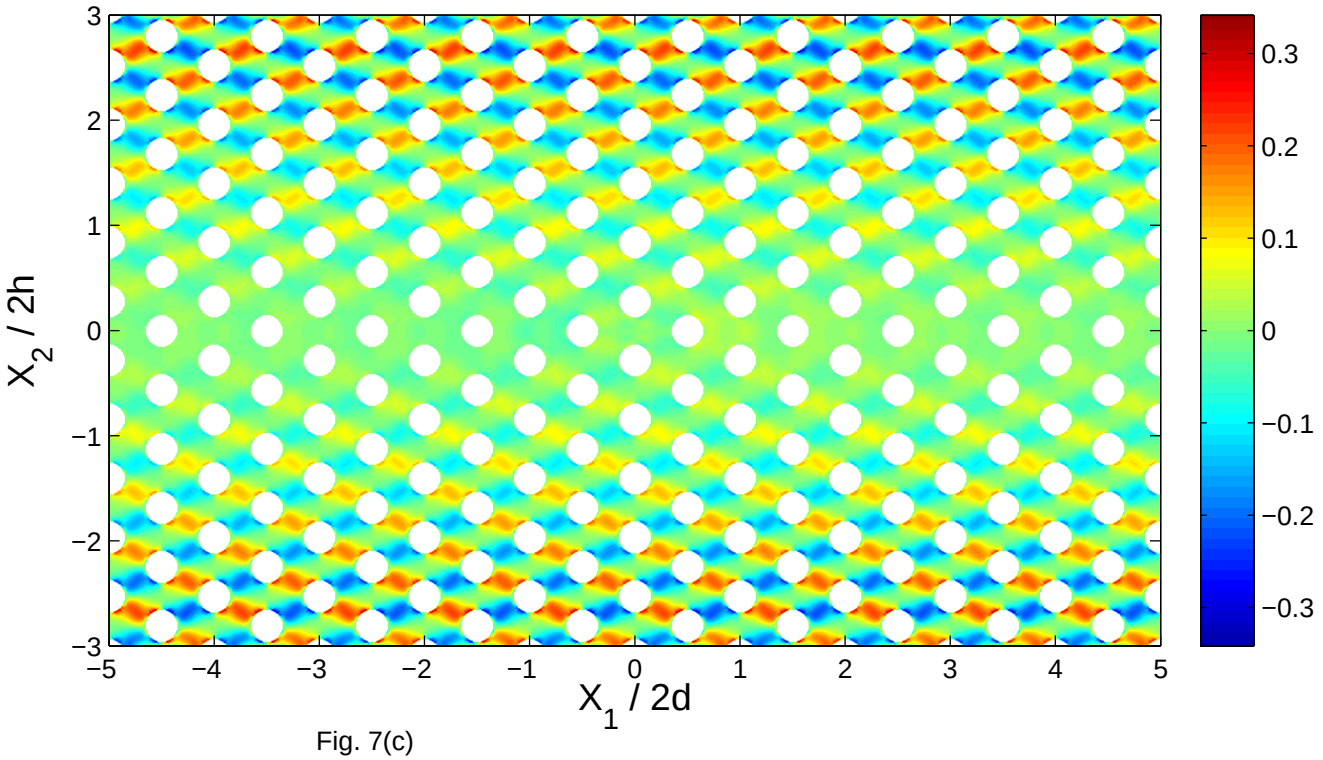

Fig. 7(c)

Preprints (www.preprints.org) | NOT PEER-REVIEWED | Posted: 25 May 2017 doi:10.20944/preprints201705.0182.v1

Peer-reviewed version available at *J. Compos. Sci.* **2017**, *1*, , 4; doi:10.3390/jcs1010004

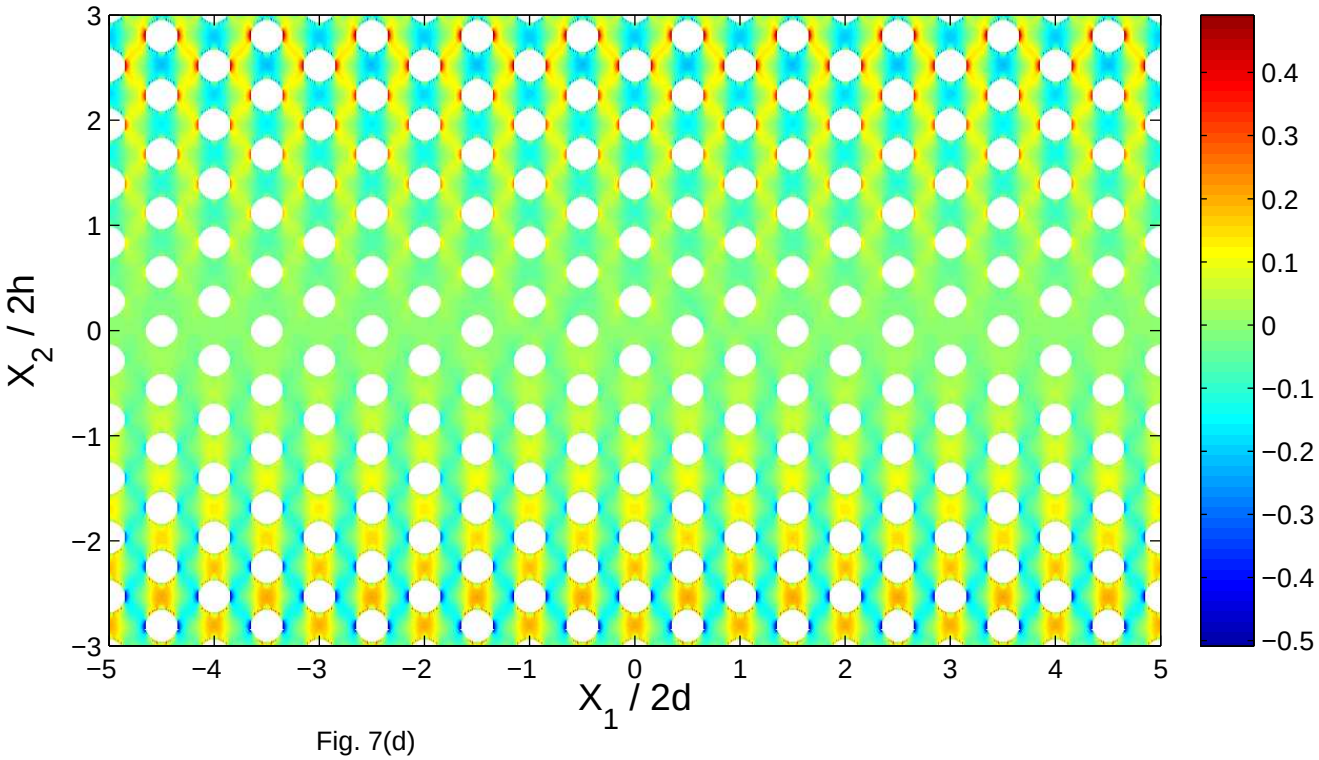

Fig. 7(d)

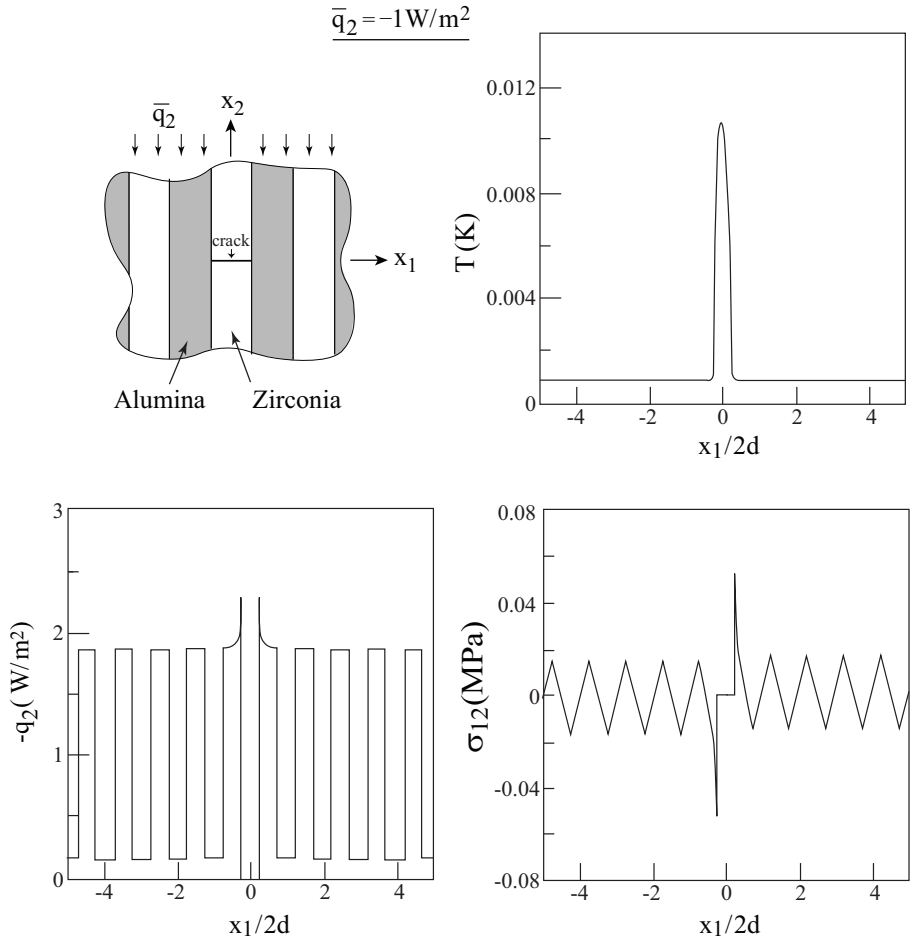

Fig.8

Preprints (www.preprints.org) | NOT PEER-REVIEWED | Posted: 25 May 2017 doi:10.20944/preprints201705.0182.v1

Peer-reviewed version available at *J. Compos. Sci.* **2017**, *1*, , 4; doi:10.3390/jcs1010004

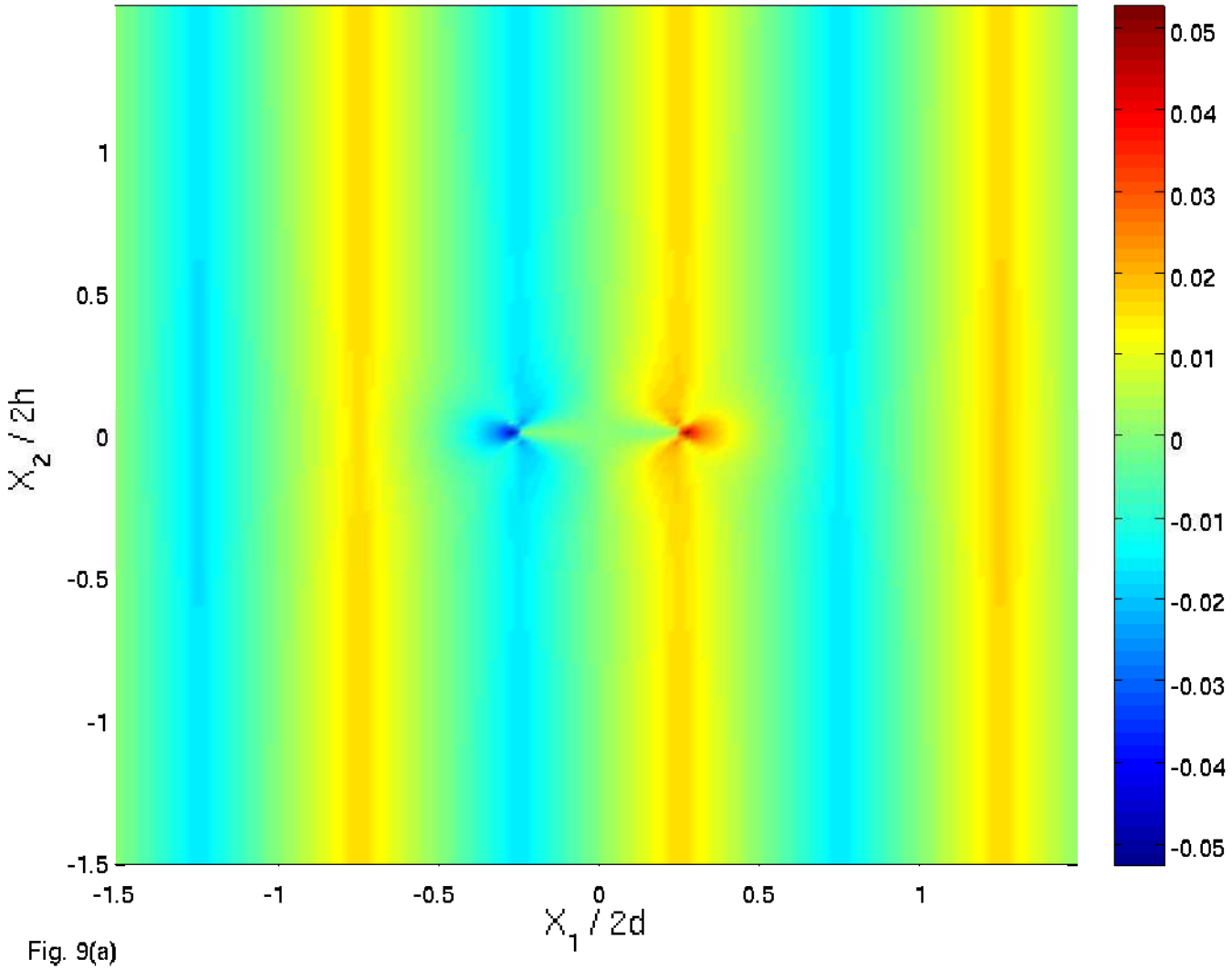

Fig. 9(a)

Preprints (www.preprints.org) | NOT PEER-REVIEWED | Posted: 25 May 2017 doi:10.20944/preprints201705.0182.v1

Peer-reviewed version available at *J. Compos. Sci.* **2017**, *1*, , 4; doi:10.3390/jcs1010004

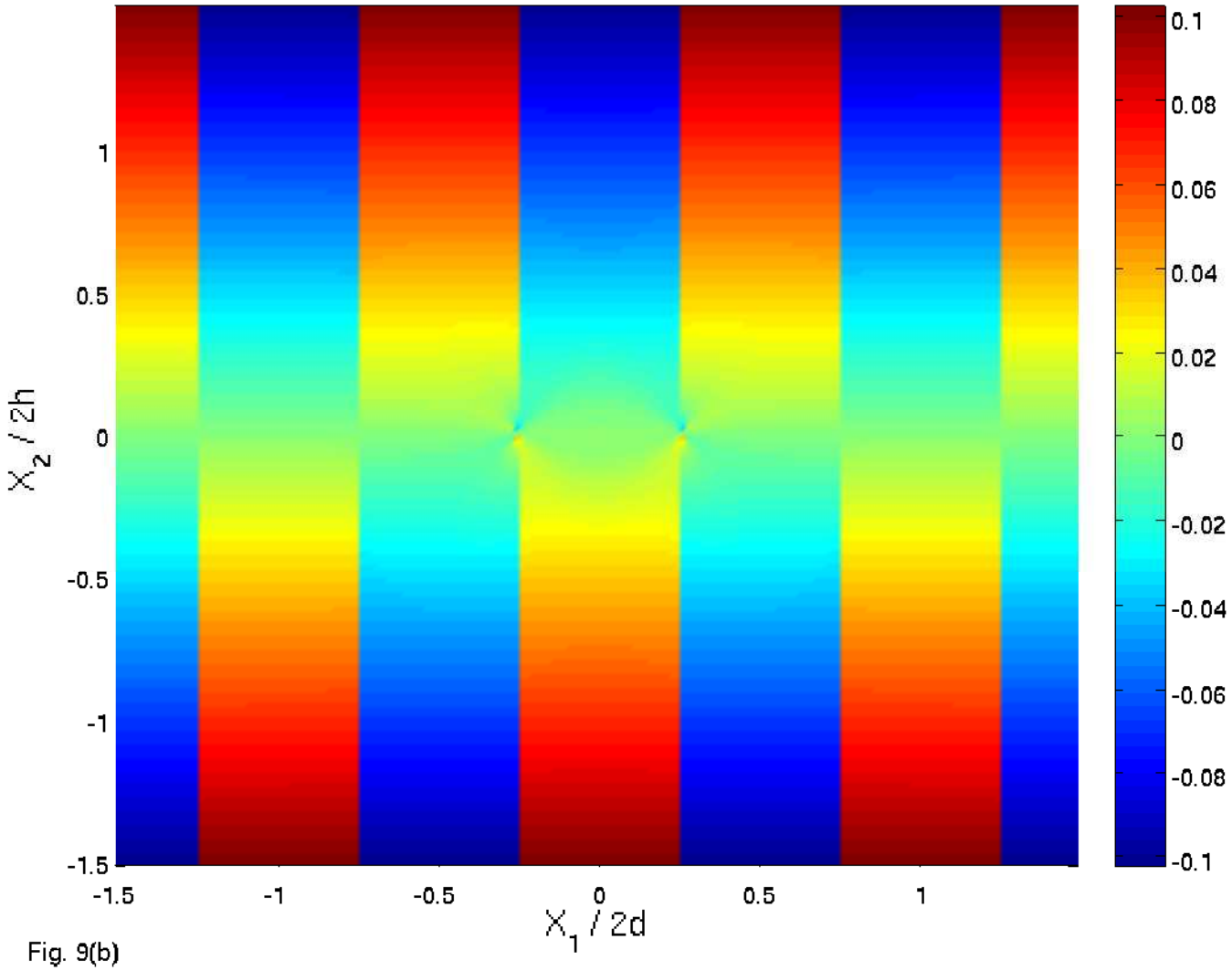

Fig. 9(b)